Nuclear Engineering and Technology 55 (2023) 4664–4670

Contents lists available at ScienceDirect

Nuclear Engineering and Technology

journal homepage: www.elsevier.com/locate/net

Original Article

Production and investigation of 3D printer ABS filaments filled with some rare-earth elements for gamma-ray shielding

Batuhan Gultekin [a], Fatih Bulut [b], Hatice Yildiz [a], Hakan Us [a], Hasan Ogul [a,*]

[a] Department of Nuclear Engineering, Sinop University, Sinop, Turkey
[b] Scientific and Technological Research Applications and Research Center, Sinop University, Sinop, Turkey

ARTICLE INFO

Keywords:
3D printer
radiation shielding
ABS
Rare-earth elements

ABSTRACT

Radiation is the main safety issue for almost all nuclear applications, which must be controlled to protect living organisms and the surrounding materials. In this context, radiation shielding materials have been investigated and used in nuclear technologies. The choice of materials depends on the radiation usage area, type, and energy. Polymer materials are preferred in radiation shielding applications due to their superior characteristics such as chemical inertness, resistivity, low weight, flexibility, strength, and low cost. In the presented work, ABS polymer material, which is possibly the most commonly used material in 3D printers, is mixed with Gd_2O_3 and Er_2O_3 nanoparticles. ABS filaments containing these rare-earth elements are then produced using a filament extruder. These produced filaments are used in a 3D printer to create shielding samples. Following the production of shielding samples, SEM, EDS, and gamma-ray shielding analyses (including experiments, WinXCOM, GEANT4, and FLUKA) are performed. The results show that 3D printing technology offers significant enhancements in creating homogeneous and well-structured materials that can be effectively used in gamma-ray shielding applications.

1. Introduction

"Radiation" could be an unpleasant term for many people, but its usage area is considerably wide and includes many critical fields in our lives, such as scientific, defense, medical, industrial, and nuclear power plant applications. It can be considered a major safety issue for almost all nuclear applications, as it must be controlled to protect living organisms and the surrounding materials of these applications. In this context, radiation shielding materials have been investigated and used in nuclear technologies. Here, the choice of materials needs to be based on the radiation usage area, type, and energy. Consequently, various types of shielding materials have been reported in the literature, including glass [1–3], alloys [4–6], concrete [7–9], and polymers [10–12].

The analysis presented in this paper focuses on polymers, where it's important to note that the production of polymer-based materials can be accomplished through various techniques, with "casting" and "printing" standing out as perhaps the most popular options. In fact, there are numerous published works that report the molding of novel polymer radiation shields [10–15]. It hosuld be noted here that the main drawback of the "casting" technique is that it cannot easily achieve the desired sizes and complex shapes that can be readily accomplished with 3D printers since complex shapes often require complex molds. In this regard, considering the widespread availability and well-known advantages of 3D printers, it can be safely stated that they are excellent candidates for creating radiation shielding materials. Therefore, the "printing" option was chosen as the technique for this work. There have been limited reports on the use of 3D printers to produce shielding materials. For instance, Elsafi et al. [16] printed PLA samples embedded with bismuth nanoparticles and evaluated their gamma-ray shielding performance. The authors concluded that 3D printed samples hold promise as radiation shielding materials. In another study, Jreije et al. [17] produced 3D filaments by adding TiO_2 nanoparticles and investigated their radiation shielding performance. They found that the printed ABS sample containing 5% TiO_2 particles could be used to protect electronic devices operating in a radiotherapy room from radiation. Similarly, using 3D printing technology, Viskadourakis et al. [18] examined the electromagnetic shielding effectiveness of PLA material containing graphene oxide and ABS containing carbon nanotubes. The results indicated that the 3D printing technique could be a useful option for fabricating alternative electromagnetic shielding materials. Further

* Corresponding author.
E-mail address: hsnogul@gmail.com (H. Ogul).

https://doi.org/10.1016/j.net.2023.09.009
Received 4 July 2023; Received in revised form 23 August 2023; Accepted 6 September 2023
Available online 21 September 2023
1738-5733/© 2023 Korean Nuclear Society. Published by Elsevier B.V. This is an open access article under the CC BY-NC-ND license (http://creativecommons.org/licenses/by-nc-nd/4.0/).

Table 1
The composition of the samples.

Sample Code	ABS (%)	Gd_2O_3 (%)	Er_2O_3 (%)	Density (g/cm^3)
ABS-0	100	0	0	1.0442
ABS-Gd5	95	5	0	1.0756
ABS-Er5	95	0	5	1.0768
ABS-Gd10	90	10	0	1.1261
ABS-Er10	90	0	10	1.1289
ABS-Gd20	80	20	0	1.2428
ABS-Er20	80	0	20	1.2490

studies on this topic can be found in Refs. [19–22].

In this study, the base material is ABS, and the chosen additives are rare-earth compounds: Gd_2O_3 and Er_2O_3. There is already some radiation shielding studies on rare-earth elements [23,24]. However, there is no study reported on the chosen base material and additives. Among the selected additives, Gd_2O_3, specifically the gadolinium (Gd) element, possesses the highest thermal neutron absorption cross section among all elements. It is commonly used in nuclear reactor control rods for effective fission distribution, making it advantageous for shielding thermal neutrons. The neutron shielding capacities of these additives are well-documented in the literature, and it is worth investigating their gamma-ray shielding performance as well. Additionally, it is known that gadolinium-containing contrast agents are administered to patients to enhance image contrast in magnetic resonance (MR) devices, which are imaging techniques used in the field of nuclear medicine. Hence, the use of gadolinium-based additives can be considered more appropriate in terms of human health compared to the toxic components mentioned in the literature [25]. The other additive, Er_2O_3, contains the erbium (Er) element, which is utilized in neutron absorbing control rods in nuclear technology [26,27]. Furthermore, both Gd and Er elements are expected to contribute positively to gamma-ray shielding due to their high atomic numbers. The choice of oxide forms as additives instead of using Gd and Er directly is due to the tendency of Gd and Er elements to bind nonmetals within the polymer material, which can result in the release of nonmetal gases until saturation is reached [28]. Moreover, Er_2O_3 is employed as an additive material in infrared absorber glasses and welding glasses [29]. It is important to emphasize that there is currently no literature study that investigates the combination of 3D printing technology and the mentioned rare-earth elements for gamma-ray shielding. Besides, it should be underlined that there is a design freedom with help of 3D printers. The presented study proves the capability to generate required physical forms and characteristics that would otherwise be unattainable through conventional manufacturing methods.

2. Materials and methods

In this study, the base material chosen is acrylonitrile butadiene styrene (ABS) polymer, while the additive nanoparticles used are Gd_2O_3 and Er_2O_3. ABS and poly lactic acid (PLA) are the most commonly used commercial polymers in 3D printers. ABS offers several advantages over PLA, including easier printability [30], superior mechanical properties [21], and a higher melting temperature [21]. These properties make ABS more durable and suitable for use at higher temperatures. Therefore, ABS was chosen for this work. Additionally, the main motivation on choosing nanoparticle size additives relies on the fact that filling the polymers with nanoparticles results in higher density compare to the micron sized ones [10]. The production of filaments with the desired mass ratios of the additives was carried out using a filament extruder machine as the first step. Subsequently, test samples were printed using a 3D printer. To evaluate the surface morphology of the prepared test samples, SEM/EDS measurements were conducted. Gamma-ray shielding tests were then performed as described below.

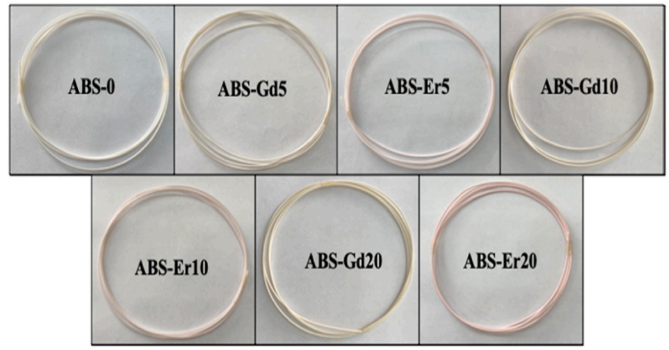

Fig. 1. The fabricated filaments.

Fig. 2. The pictures of the printed samples.

2.1. Filament and sample production

The used additives, Gd_2O_3 nanopowder (99.95% purity, particle size: 95 nm), and Er_2O_3 nanopowder (99.95% purity, particle size: 110 nm), were purchased from Nanografi Company (Türkiye), while ABS granules were obtained from RIIZ Company (Türkiye). A twin-screw extruder (Gulnar Machines, Turkey: screw diameter 16 mm, L/D = 40) was used to fabricate the filaments described in Table 1. It should be noted here that ABS granules and the selected nanopowders were dried in an oven at 100 °C for 12 h before the production. The pictures of the produced filaments are shown in Fig. 1.

Then, the filaments were used to print the shielding material samples in the sizes of 10 mm thickness and 20 mm diameter with help of an 3D printer (Creality CR-10 Smart Pro 3D Direct Drive). The pictures of the printed samples are given in Fig. 2. The average densities of the printed samples are calculated using the Archimedes method [31]. In short, the

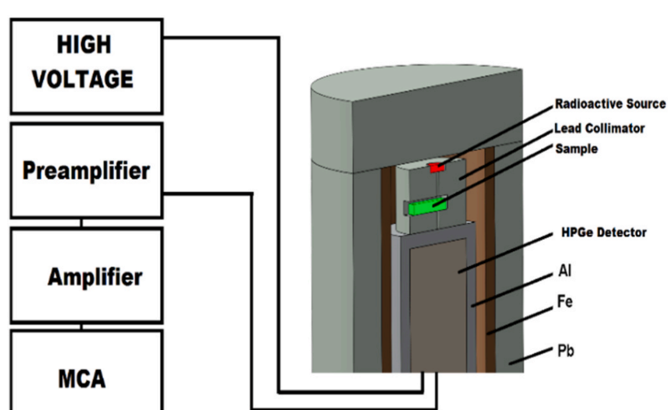

Fig. 3. The design of the gamma-ray shielding tests.

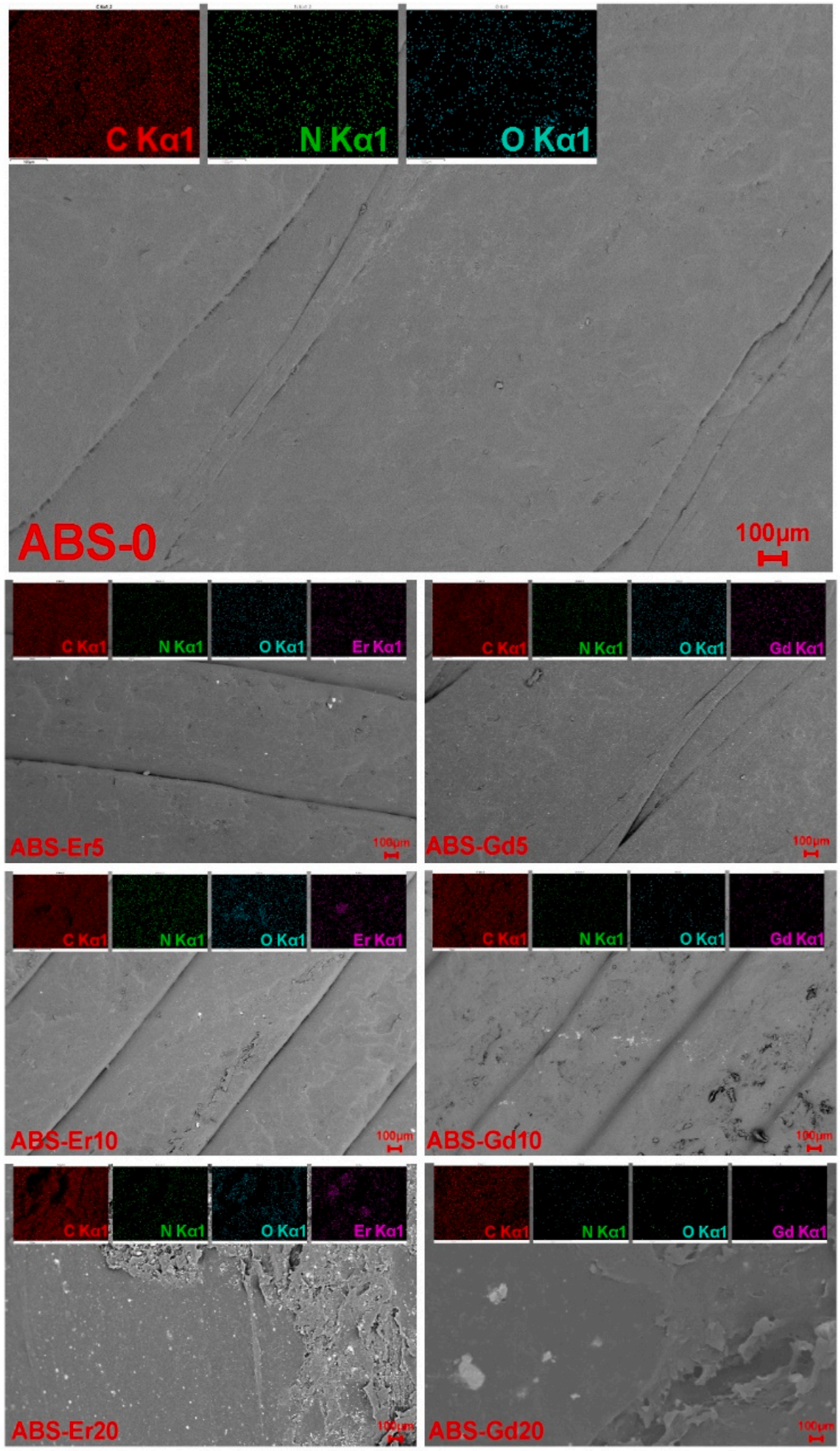

Fig. 4. The SEM images and EDS mapping results of the samples. All graphs are shown at 100 μm scale.

given densities in Table 1 are obtained using the following equation.

$$\rho = \frac{A}{A - B}\rho_W \quad (1)$$

where A and B define the weight of the polymer in the air and water, respectively, while ρ_W corresponds to the density of water.

2.2. Gamma-ray shielding tests

Gama-ray shielding tests are conducted on experimental measurements (HPGe detector system), theoretical calculations (WinXCOM [32]) and Monte Carlo (MC) simulations (GEANT4 [33] and FLUKA [34]). 10.7.2 version of GEANT4 is used while FLUKA (2021.2.9) is interfaced with Flair 3.1. The details about experimental apparatus, MC

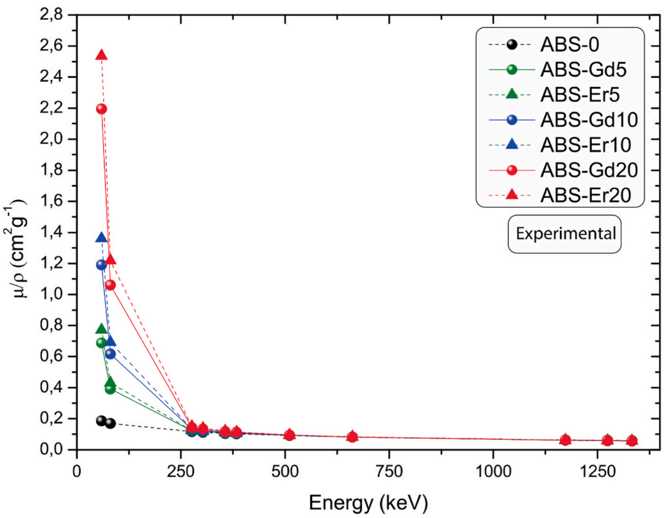

Fig. 5. Comparison of MAC results for the printed samples.

simulations and radiation sources are given in Reference [14]. Shortly, the experimental design of the gamma-ray shielding tests is illustrated in Fig. 3. The distance between the radioactive source and the sample is 3 cm, while the distance between the sample and the detector is 3.9 cm. The used point sources could be listed as follows: ^{241}Am (59.5 keV), ^{133}Ba (80.9, 276.3, 302.8, 356.0 and 383.8 keV), ^{22}Na (511.0 and 1274.5 keV), ^{137}Cs (661.6 keV), and ^{60}Co (1173.2 and 1332.5 keV). The obtained radiation density peaks were analyzed using MAESTRO program. The same gamma-ray energies and designs are modeled in MC simulations, and then the codes are executed. Here, 10 000 000 gamma particles are simulated and sent over the modeled test sample. Both simulation programs provide the density of the incident and transmitted radiation.

The considered gamma-ray shielding parameters could be listed as mass attenuation coefficient (MAC), half value layer (HVL), and radiation protection efficiency (RPE). The formula of the considered parameters are given below.

$$\mathrm{MAC} = \mu \Big/ \rho = \left(-\frac{\ln \frac{I}{I_0}}{x} \right) \Big/ \rho \tag{2}$$

$$\mathrm{HVL} = \frac{\ln(2)}{\mu} \tag{3}$$

$$\mathrm{RPE} = \left(1 - \frac{I}{I_0} \right) 100 \tag{4}$$

where I_0, I, x, ρ, and μ stand for the incident radiation density, the transmitted radiation density, the shielding material thickness, the shielding material density and linear attenuation coefficient.

Table 2
Experimental HVL values of the printed samples in unit of cm.

Energy (keV)	Sample	Experiment	WinXCOM	GEANT4	FLUKA	Energy (keV)	Sample	Experiment	WinXCOM	GEANT4	FLUKA
59.5	ABS-0	3.6786	3.5216	3.6996	3.5301	**511**	ABS-0	7.4131	7.1194	7.0995	7.0995
	ABS-Er5	0.8299	0.8167	0.8472	0.8200		ABS-Er5	7.3610	6.8217	6.8258	6.8258
	ABS-Er10	0.4739	0.4424	0.4581	0.4475		ABS-Er10	6.6980	6.4308	6.4559	6.4308
	ABS-Er20	0.2021	0.2145	0.2219	0.2150		ABS-Er20	6.0672	5.6799	5.7384	5.6898
	ABS-Gd5	0.9573	0.9189	0.9490	0.9188		ABS-Gd5	7.4131	6.8569	6.8587	6.8624
	ABS-Gd10	0.4775	0.4467	0.5222	0.5109		ABS-Gd10	6.8303	6.4490	6.5200	6.5042
	ABS-Gd20	0.2629	0.2490	0.2561	0.2489		ABS-Gd20	6.2518	5.7993	5.8509	5.8029
80.9	ABS-0	4.0785	3.8437	3.9609	3.8482	**661.6**	ABS-0	7.8628	7.9651	7.9219	7.9461
	ABS-Er5	1.4636	1.4623	1.5111	1.4623		ABS-Er5	7.8628	7.6998	7.6753	7.6998
	ABS-Er10	0.9353	0.8675	0.8971	0.8770		ABS-Er10	7.9426	7.3218	7.3150	7.3150
	ABS-Er20	0.4874	0.4465	0.4620	0.4463		ABS-Er20	6.5369	6.5764	6.6156	6.5764
	ABS-Gd5	1.6161	1.6110	1.6697	1.6693		ABS-Gd5	8.0239	7.7277	7.7013	7.7363
	ABS-Gd10	0.9227	0.8750	1.0186	1.0221		ABS-Gd10	7.5219	7.3403	7.3668	7.3403
	ABS-Gd20	0.5538	0.5154	0.5357	0.5154		ABS-Gd20	6.1417	6.6768	6.6937	6.6768
276.3	ABS-0	6.0257	5.5924	5.6394	5.5924	**1173.2**	ABS-0	11.3344	10.4571	10.4128	10.4128
	ABS-Er5	5.2173	5.0526	5.1328	5.0561		ABS-Er5	10.6217	10.1964	10.1613	10.2152
	ABS-Er10	4.8851	4.5115	4.6124	4.5126		ABS-Er10	9.8733	9.7788	9.7544	9.7788
	ABS-Er20	3.7563	3.6131	3.7365	3.6202		ABS-Er20	9.4286	8.9383	8.9305	8.9383
	ABS-Gd5	5.5148	5.1307	5.2065	5.1322		ABS-Gd5	11.0384	10.2174	10.1814	10.2364
	ABS-Gd10	4.7630	4.5261	4.7409	4.6434		ABS-Gd10	10.1112	9.8034	9.7959	9.8421
	ABS-Gd20	4.0013	3.8043	3.9281	3.8051		ABS-Gd20	9.5361	9.0187	9.0206	9.0187
302.8	ABS-0	6.2828	5.7874	5.8219	5.7874	**1274.5**	ABS-0	10.8368	10.9126	10.8687	10.9255
	ABS-Er5	5.5359	5.3023	5.3731	5.3023		ABS-Er5	10.8368	10.6449	10.6098	10.6449
	ABS-Er10	5.1449	4.7969	4.8890	4.8161		ABS-Er10	9.4664	10.2148	10.1885	10.2148
	ABS-Er20	3.8968	3.9277	4.0462	3.9277		ABS-Er20	8.7251	9.3431	9.3346	9.3346
	ABS-Gd5	5.7907	5.3701	5.4376	5.4152		ABS-Gd5	11.1032	10.6655	10.6298	10.6789
	ABS-Gd10	4.9968	4.8128	5.0041	4.8128		ABS-Gd10	9.6710	10.2388	10.2303	10.2303
	ABS-Gd20	4.1477	4.1099	4.2254	4.1099		ABS-Gd20	9.2700	9.4241	9.4105	9.4363
356	ABS-0	6.5254	6.1521	6.1710	6.1596	**1332.5**	ABS-0	11.4426	11.1641	11.1253	11.1641
	ABS-Er5	5.8305	5.7525	5.8007	5.7575		ABS-Er5	10.5794	10.8917	10.8614	10.9132
	ABS-Er10	5.6398	5.2932	5.3686	5.3686		ABS-Er10	9.8339	10.4530	10.4312	10.4312
	ABS-Er20	4.1884	4.4756	4.5798	4.4794		ABS-Er20	9.3909	9.5653	9.5590	9.5653
	ABS-Gd5	5.7845	5.8055	5.8519	5.8055		ABS-Gd5	10.9946	10.9130	10.8815	10.9130
	ABS-Gd10	5.4810	5.3111	5.4634	5.4440		ABS-Gd10	10.1935	10.4793	10.4731	10.4793
	ABS-Gd20	4.6652	4.6360	4.7356	4.6399		ABS-Gd20	9.6075	9.6457	9.6352	9.6457
383.8	ABS-0	6.2143	6.3341	6.3462	6.3429						
	ABS-Er5	5.6074	5.9657	6.0035	5.9657						
	ABS-Er10	5.7006	5.5266	5.5900	5.5266						
	ABS-Er20	4.4879	4.7272	4.8226	4.7272						
	ABS-Gd5	6.4449	6.0113	6.0497	6.0113						
	ABS-Gd10	5.9987	5.5456	5.6770	5.6191						
	ABS-Gd20	4.8114	4.8751	4.9681	4.8751						

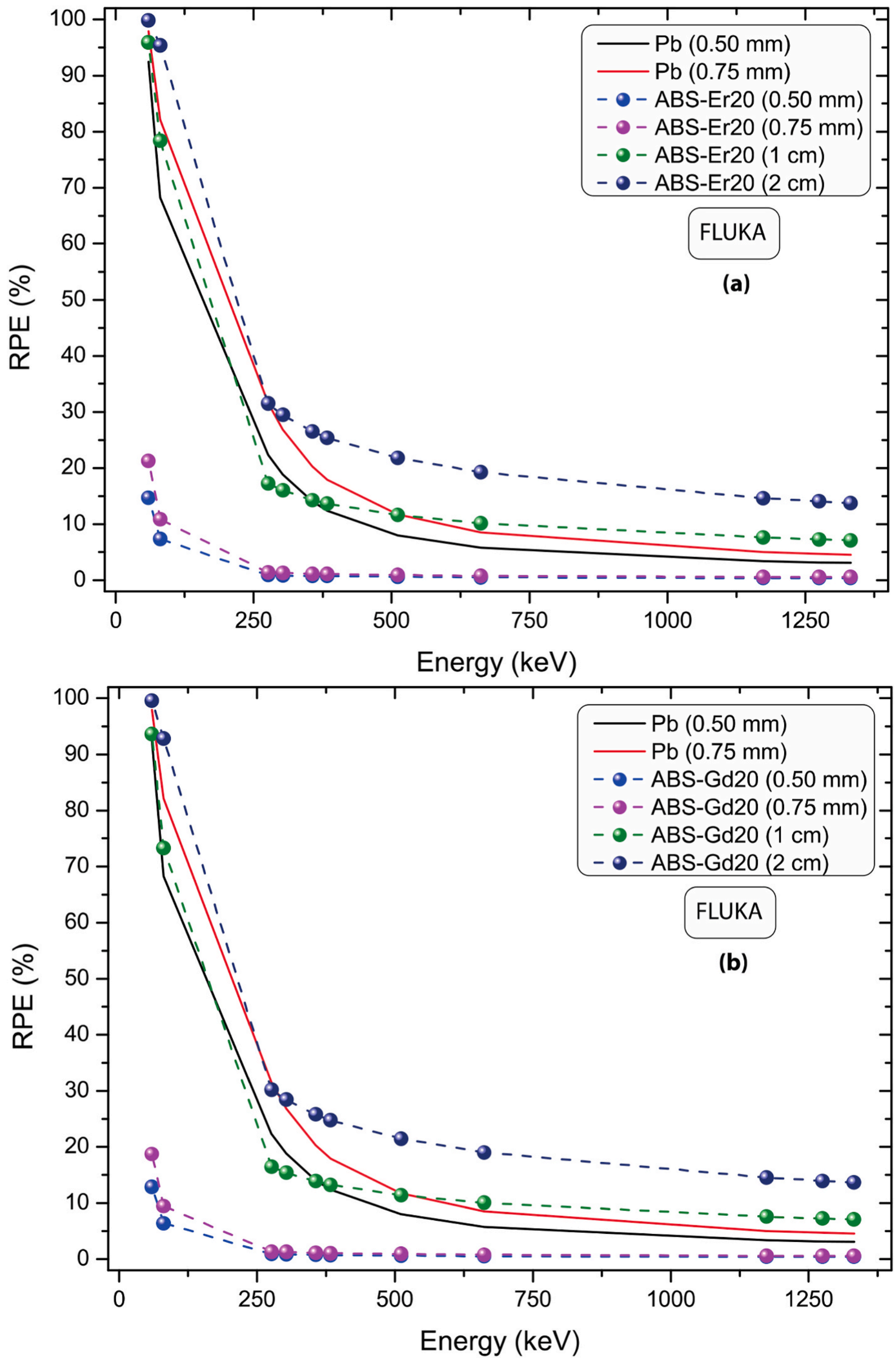

Fig. 6. RPE graphs for comparison of commercial aprons and the printed polymers ABS-Er20 (a) and ABS-Gd20 (b).

3. Results and discussion

In the presented work, ABS polymer material was mixed with some earth-rare elements, and then, 3D printer filaments were produced. The produced filaments were used to print radiation shielding test samples. SEM and EDS analyses were carried out in order to examine the surface morphology of the samples produced using a 3D printer and the distribution of the additive element in the material. In this process, the samples were coated with gold-palladium so that images can be taken with the JEOL, JSM-5300 electron microscope. SEM images were taken at 100X magnification and the EDS mapping method was preferred to obtain data from the entire sample surface. In the SEM images given in Fig. 4, it is clear that there is no indication of any impurity on the surface of the pure ABS sample. The sample surface is smooth due to the printing quality and including no additive. There are only printing lines on the surface which is quite normal in 3D printing technology. It is a remarkable result that they are at a printable level in all additive ratios. Fig. 2 and the SEM images presented in Fig. 4 show that there are excellent printing quality and well-structured ABS samples. In Fig. 4, besides the SEM images for each sample, the EDS mapping results are also included. The additive element (both Er and Gd) is given in purple color and it is clearly seen that it is homogeneously distributed on the surface. It can be concluded that the doped sample production is carried out successfully since there is no occurrence of the additive element agglomeration on the sample surfaces.

The considered first gamma-ray shielding parameter is the mass attenuation coefficient. Fig. 5 illustrates the experiment results as a function of the gamma-ray energy. It is clearly seen that the MAC values exponentially decrease with the increase of the energy. ABS-Er20 sample found to be the best gamma-ray attenuator which is followed by ABS-Gd20 sample. In other words, the addition of nanopowders enhance the gamma-ray shielding performance of the pure ABS polymer. It is safe to state that the gamma-ray shielding performance of the pure ABS is about 18 times increased by addition of 20% Er_2O_3 at 59.5 keV while it is about 1.2 times improved at 661.6 keV and 1332.5 keV. The impacts of the additives on the shielding ability are decreased with the gamma-ray energy increase and gets stable after a point.

Another gamma-ray shielding parameter considered in the presented work is the HVL. HVL describes the material thickness that reduce the initial radiation intensity to its half. Mathematical formulation is given earlier. Smaller HVL.

means better gamma-ray shielding. Therefore, in the results of HVL values, we could find the samples with smaller HVL value in order to classify it as the better gamma-ray attenuator among the considered shielding materials. Table 2 presents the experimental HVL values for all considered samples. The outcome of the HVL values are the same with MAC results: the best gamma attenuators are ABS-Er20 and ABS-Gd20. Additionally, the table provides WinXCOM, GEANT4 and FLUKA results. It seen that there is remarkable agreement between experimental result, theoretical calculation and MC simulations. The maximum deviation is about 7%. The HVL values of ABS-Er20 and ABS-Gd20 at 661.6 keV could be further compared to some commercial polymers. This energy is chosen since it is very commonly used in many work and matches with our energy selection. The HVL values of ABS-Er20 and ABS-Gd20 is given as 6.7106 cm and 6.8131 cm in the presented table. Unsaturated polyester [35], polyphenylenesulfide [36], polyacrylonitrile [36], polyamide [34], polyvinylidenechloride [36] and ABS [22] are reported as 6.9866 cm, 6.5329 cm, 6.9107 cm, 7.1010 cm, 5.7660 cm and 8.1210 cm, respectively.

The last parameter considered here is the radiation protection efficiency. RPE calculations are made for all energy bins considered in the presented work. Although a very wide range of gamma-ray energy is considered in the presented work, here, we would like to focus on possible usage area of the printed shielding material. Aprons will be considered here. Most of the current commercial aprons are made of lead, and they have disadvantages such as being expensive, heavy, and ineffective against scattered internal radiation [37]. Therefore, there is a great effort on finding lead free aprons. The commercial lead aprons are fabricated in two different lead thickness: 0.50 mm and 0.75 mm. In order to compare our samples with current commercial aprons, Fig. 6 is prepared using FLUKA simulation program. Here, it is seen that if ABS-Er20 or ABS-Gd20 apron produced with thickness of 2 cm have similar gamma-ray protection with lead aprons at low gamma-ray energy region that is valid energy region for medical applications and x-ray laboratories. We could go one more step further by comparing the weight of the polymer and lead aprons. The commercial aprons are fabricated in two different sizes: medium and large [38]. The surface area of the large size apron is about 5999.4680 cm^2 while medium size is 5218.4856 cm^2 [38]. The weights of large size with 0.50 mm and 0.75 mm are 6.803 kg and 10.205 kg, respectively, while the weights of the medium size apron are 5.917 kg and 8876 kg [38]. 2 cm thickness of ABS-Er20 or ABS-Gd20 samples ensure the same shielding effectiveness with 2.951 kg and 1.778 kg for large size, respectively. On the other hand, the weights for medium size are 2.280 kg and 1.456 kg. The obtained new shielding materials are very light compared to the commercial lead aprons.

4. Conclusion

In the presented study, ABS filaments were modified by incorporating rare-earth element nanoparticles. These modified filaments were then used in a 3D printer to create shielding test samples. SEM and EDS analyses revealed that the ABS samples exhibited homogeneity and well-defined structures. Notably, all produced filaments were found to be suitable for printing in the desired additive ratios. Gamma-ray shielding tests were conducted to evaluate the performance of the printed samples. The experimental, theoretical, and simulation results exhibited a remarkable agreement, demonstrating that increasing the amount of additives in the polymer composites enhanced the gamma-ray shielding effectiveness. RPE calculations indicated that the printed ABS-Er20 aprons could serve as excellent alternatives to commercial aprons in medical applications and x-ray laboratories. In essence, 3D printers offer a valuable tool for the manufacturing community to fabricate lightweight shielding materials, whether in complex or simple shapes, with lower material costs and desired characteristics. The obtained results hold promise for future applications and warrant further investigation, including mechanical testing, to comprehensively assess the performance of these materials.

Declaration of competing interest

The authors declare that they have no known competing financial interests or personal relationships that could have appeared to influence the work reported in this paper.

Acknowledgements

This study was funded by the Scientific and Technological Research Council of Türkiye (TUBITAK) 1002-A Grant No 122M736.

References

[1] M.S. Al-Buriahi, Z.A. Alrowaili, C. Eke, J.S. Alzahrani, I.O. Olarinoye, C. Sriwunkum, Optical and radiation shielding studies on tellurite glass system containing ZnO and Na2O, Optik 257 (2022), 168821.

[2] B. Aktas, A. Acikgoz, D. Yilmaz, S. Yalcin, K. Dogru, N. Yorulmaz, The role of TeO2 insertion on the radiation shielding, structural and physical properties of borosilicate glasses, J. Nucl. Mater. 563 (2022), 153619.

[3] H.A. Esawii, E. Salama, L. Sayed El-ahll, M. Moustafa, H.M. Saleh, High impact tungsten-doped borosilicate glass composite for gamma and neutron transparent radiation shielding, Prog. Nucl. Energy 150 (2022), 104321.

[4] M.F. Turhan, F. Akman, A. Taşer, K. Dilsiz, H. Oğul, M.R. Kaçal, O. Agar, Gamma radiation shielding performance of CuxAg(1-x)-alloys: experimental, theoretical and simulation results, Prog. Nucl. Energy 143 (2022), 104036.

[5] H. Yaykaşlı, H. Eskalen, Y. Kavun, M. Gögebakan, Microstructural, thermal, and radiation shielding properties of $Al_{50}B_{25}Mg_{25}$ alloy prepared by mechanical alloying, J. Mater. Sci. Mater. Electron. 33 (2022) 2350–2359.

[6] R. Bagheri, H.F. Rad, H. Ranjbar, Radiation shielding studies of low melting point MCP alloys in the photon energy range of 10 keV–10 MeV, Ann. Nucl. Energy 181 (2023), 109525.

[7] A. Ardiansyah, D. Tahir, H. Heryanto, B. Armynah, H. Salah, A. Sulieman, D. A. Bradley, Science mapping for concrete composites as radiation shielding: a review, Radiat. Phys. Chem. 207 (2023), 110835.

[8] T. Daungwilailuk, C. Yenchai, W. Rungjaroenkiti, P. Pheinsusom, C. Panwisawas, W. Pansuk, Use of barite concrete for radiation shielding against gamma-rays and neutrons, Construct. Build. Mater. 326 (2022), 126838.

[9] A. Öz, B. Bayrak, E. Kavaz, G. Kaplan, O. Çelebi, H.G. Alcan, A.C. Aydın, The radiation shielding and microstructure properties of quartzic and metakaolin based geopolymer concrete, Construct. Build. Mater. 342 (Part B) (2022), 127923.

[10] H. Oğul, O. Agar, F. Bulut, M.R. Kaçal, K. Dilsiz, H. Polat, F. Akman, A comparative neutron and gamma-ray radiation shielding investigation of molybdenum and boron filled polymer composites, Appl. Radiat. Isot. 194 (2023), 110731.

[11] M.I. Sayyed, S. Yasmin, N. Almousa, M. Elsafi, The radiation shielding performance of polyester with TeO2 and B2O, Processes 10 9 (2022) 1725.

[12] M.I. Abbas, A.H. Alahmadi, M. Elsafi, S.A. Alqahtani, S. Yasmin, M.I. Sayyed, M. M. Gouda, A.M. El-Khatib, Effect of kaolin clay and ZnO-nanoparticles on the radiation shielding properties of epoxy resin composites, Polymers 14 22 (2022) 4801.

[13] O. Kilicoglu, C.V. More, F. Akman, K. Dilsiz, H. Oğul, M.R. Kaçal, H. Polat, O. Agar, Micro Pb filled polymer composites: theoretical, experimental and simulation results for γ-ray shielding performance, Radiat. Phys. Chem. 194 (2022), 110039.

[14] H. Oğul, H. Polat, F. Akman, M.R. Kaçal, K. Dilsiz, F. Bulut, O. Agar, Gamma and Neutron Shielding Parameters of Polyester-based composites reinforced with boron and tin nanopowders, Radiat. Phys. Chem. 201 (2022), 110474.

[15] P. Gong, M. Ni, H. Chai, F. Chen, X. Tang, Preparation and characteristics of a flexible neutron and γ-ray shielding and radiation-resistant material reinforced by benzophenone, Nucl. Eng. Technol. 50 (3) (2018) 470–477.

[16] M. Elsafi, M.A. El-Nahal, M.I. Sayyed, G. Saleh, M.I. Abbas, Novel 3-D printed radiation shielding materials embedded with bulk and nanoparticles of bismuth, Sci. Rep. 12 (2022), 12467.
[17] A. Jreije, S. K. Mutyala, B. G. Urbonavičius, A. Šablinskaitė, N. Keršienė, J. Puišo, Z. Rutkūnienė, D. Adlienė. Modification of 3D printable polymer filaments for radiation shielding application, Polymers, 15(7), 2023, 1700..
[18] Z. Viskadourakis, K.C. Vasiolopoulos, E.N. Economou, C.M. Soukoulis, G. Kenanakis, Electromagnetic shielding effectiveness of 3D printed polymer composites, Appl. Phys. A 123 (2017) 736.
[19] B. Gultekin, H. Ogul, Evaluation of Acrylonitrile Butadiene Styrene (ABS) polymer reinforced with Bi and TiO2 nanopowders for gamma and neutron shielding, Radiochim. Acta 111 (2) (2022) 137–145.
[20] M. Alssabbagh, A.A. Tajuddina, M. Abdulmanap, R. Zainon, Evaluation of 3D printing materials for fabrication of a novel multi-functional 3D thyroid phantom for medical dosimetry and image quality, Radiat. Phys. Chem. 135 (2017) 106–112.
[21] S. Woosley, N.A. Galehdari, A. Kelkar, S. Aravamudhan, Fused deposition modeling 3D printing of boron nitride composites for neutron radiation shielding, Journal of Mater. Res. 33 (2018) 3657–3664.
[22] H. Ogul, Radiation attenuation properties of polymer composites mixed with tantalum carbide, Radiat. Eff. Defect Solid 177 (2022) 5–6.
[23] R.B. Malidarre, I. Akkurt, O. Kocar, I. Ekmekci, Analysis of radiation shielding, physical and optical qualities of various rare earth dopants on barium tellurite glasses: a comparative study, Radiat. Phys. Chem. 207 (2023), 110823.
[24] M.Y. A Mostafa, H.M.H. Zakaly, S.A.M. Issa, H.A. Saudia, A.M.A. Henaish, Tailoring variations in the linear optical and radiation shielding parameters of PVA polymeric composite films doped with rare-earth elements, Appl. Phys. A 128 (2022) 199.
[25] S. Sarkar, Z. Vinokur, C. Xu, T. Soloviova, A. Shahbaz, A. Gjoni, Mapping gadolinium contrast in a complex ionic and photosynthesis environment of pineapple by near-infrared and X-ray imaging, Spectrosc. Lett. 53 (7) (2020) 505–511.
[26] J.R. Lamarsh, A.J. Baratta, Introduction to Nuclear Engineering, vol. 3, Prentice hall, Upper Saddle River, NJ, 2001, p. 783.
[27] K.S. Mann, A. Rani, M.S. Heer, Shielding behaviors of some polymer and plastic materials for gamma-rays", Radiat. Phys. Chem. 106 (2015) 247–254.
[28] S. Obregón, A. Kubacka, M. Fernández-García, G. Colón, High-performance Er3+–TiO2 system: dual up-conversion and electronic role of the lanthanide, J. Catal. 299 (2013) 298–306.
[29] N. Effendy, Z.A. Wahab, S.H. Abdul Aziz, K.A. Matori, M.H.M. Zaid, S.S.A. Rashid, Characterization and optical properties of erbium oxide doped ZnO–SLS glass for potential optical and optoelectronic materials, Materials Express 7 (1) (2017) 59–65.
[30] A. Olsson, M.S. Hellsing, A.R. Rennie, New possibilities using additive manufacturing with materials that are difficult to process and with complex structures, Phys. Scripta 92 (2017), 053002.
[31] M.E. Mahmoud, A.M. El-Khatib, M.S. Badawi, A.R. Rashad, R.M. El-Sharkawy, A. A. Thabet, Fabrication, characterization and gamma rays shielding properties of nano and micro lead oxide-dispersed-high density polyethylene composites, Radiat. Phys. Chem. 145 (2018 160–173).
[32] L. Gerward, N. Guilbert, K. Jensen, H. Levring, WinXCom - a program for calculating X-ray attenuation coefficients, Radiat. Phys. Chem. 71 (2004) 653–654.
[33] S. Agostinelli, J. Allison, K. Amako, J. Apostolakis, H. Araujo, P. Arce, M. Asai, D. Axen, S. Banerjee, G. Barrand, F. Behner, L. Bellagamba, J. Boudreau, L. Broglia, A. Brunengo, H. Burkhardt, S. Chauvie, J. Chuma, R. Chytracek, G. Cooperman, Geant4-a simulation toolkit, Nucl. Instrum. Methods Phys. Res. 506 (2003) 250–303.
[34] T.T. Böhlen, F. Cerutti, M.P.W. Chin, A. Fassò, A. Ferrari, P.G. Ortega, A. Mairani, P.R. Sala, G. Smirnov, V. Vlachoudis, The FLUKA code: developments and challenges for high energy and medical applications, Nucl. Data Sheets 120 (2014) 211–214.
[35] F. Özkalaycı, M.R. Kaçal, O. Agar, H. Polat, A. Sharma, F. Akman, Lead(II) chloride effects on nuclear shielding capabilities of polymer composites, J. Phys. Chem. Solid. 145 (2020), 109543.
[36] M.R. Kaçal, F. Akman, M.I. Sayyed, Evaluation of gamma-ray and neutron attenuation properties of some polymers, Nucl. Eng. Technol. 51 (3) (2019) 818–824.
[37] G. Crane, P. Abbott, Radiation shielding in dentistry: an update, Aust. Dent. J. 61 (2016) 277–281.
[38] Web site: https://infabcorp.com/standard-sizing-charts, access date: June.23.2023.